ELSEVIER

Journal of Chromatography A, 944 (2002) 23–39

JOURNAL OF CHROMATOGRAPHY A

www.elsevier.com/locate/chroma

Solvent gradient operation of simulated moving beds I. Linear isotherms

Stefanie Abel, Marco Mazzotti, Massimo Morbidelli*

ETH Zürich, Institut für Verfahrenstechnik, Sonneggstrasse 3, CH-8092 Zürich, Switzerland

Abstract

The simulated moving bed (SMB) is a multi-column chromatographic separation process, which – with respect to the single-column preparative batch process – allows for a continuous separation with larger productivity and smaller solvent consumption at the same time. The benefits of this process have been shown for several different applications in fine chemistry, particularly for the separation of enantiomers. In general, SMBs are operated under isocratic conditions. However, separation performance can be further improved by applying some sort of gradient mode operation, in order to optimize the operating conditions of each individual section of the unit. This can be achieved by tuning the retention behavior of the solutes to be separated along the unit, namely by enforcing weak adsorption conditions in sections 1 and 2, and strong adsorption conditions in sections 3 and 4. This can be achieved by applying a temperature gradient (high temperature in section 1, and low temperature in section 4), a pressure gradient (e.g. in the supercritical SMB, when pressure is high in section 1, and low in section 4), or a solvent gradient, which is the aim of this work. In the solvent gradient mode the mobile phase consists of a mixture of two or more solvents. To different mobile phase compositions corresponds a different retention behavior of the solutes, i.e. different adsorption isotherms. In this work we study a closed loop SMB unit with solvent mixtures of two different compositions entering the unit at the feed and desorbent inlet ports, respectively. Thereby two different mobile phase compositions are established in sections 1 and 2, and sections 3 and 4, respectively. To optimize this process the equilibrium theory design criteria for non-linear SMBs are extended to describe this operation mode. It is shown how the region of separation is derived and how the optimal operating conditions can be found. Finally the solvent gradient mode is compared with the isocratic mode in terms of productivity and solvent consumption.

Keywords: Solvent gradients; Simulated moving bed chromatography; Preparative chromatography; Adsorption isotherms; Enantiomer separation; Mobile phase composition; Ionone

1. Introduction

Simulated moving beds (SMBs) are well established for the adsorption based separation of hydrocarbons as well as of fine chemicals, particularly enantiomers [1–3]. This technology covers a broad range of production scales from the laboratory units, which use chromatographic columns with a 0.5 cm internal diameter, to the multi-ton production units licensed by Novasep for chiral separations with column diameters between 20 and 100 cm, to the largest SMB unit licenced recently in South Korea by the Institute Francaise du Petrol with a column diameter of 8 m for the production of $700 \cdot 10^6$ kg per year of *p*-xylene. New applications are envisaged in

*Corresponding author. ETH Zürich, Laboraborium für Technische Chemie, Universitätstrasse 6, CH-8092 Zürich, Switzerland. Tel.: +41-1-6323-034; fax: +41-1-6321-082.

E-mail address: morbidelli@tech.chem.ethz.ch (M. Morbidelli).

0021-9673/02/$ – see front matter
PII: S0021-9673(01)01087-1

the near future, particularly in the emerging area of bio-separations, e.g. for the purification of enzymes, peptides, antibiotics and natural extracts [4].

The SMB technology is a continuous countercurrent separation process, which is in principle equivalent to the true moving bed (TMB) unit schematically drawn in Fig. 1, provided that a number of equivalence relationships are fulfilled [1]. In the SMB, the continuous movement of the solid is simulated by periodically switching the inlet and outlet ports of the unit. With reference to the TMB in Fig. 1 and a binary system under complete separation conditions, the ratio between fluid and solid flowrates in the four sections is chosen so that the more retained adsorbate A is carried by the solid-phase to the extract outlet, while the less retained adsorbate B is conveyed by the mobile phase to the raffinate port. The regeneration of the solid and fluid phase required for a continuous process is carried out in sections 1 and 4, respectively.

All the applications mentioned above are operated in the liquid phase under isocratic conditions, i.e. at constant temperature, pressure, and mobile phase composition, thus letting the components to be separated adsorb according to the same adsorption isotherm in the four sections of the unit. However, the separation of enantiomers as well as bio-separations are often based on rather small selectivities, e.g. between 1.1 and 1.2. In these cases productivity can be boosted by operating the SMB unit in the gradient mode where the conditions in each section are chosen independently in order to reduce adsorptivity and retention times in sections 1 and 2, and to increase them in sections 3 and 4.

The benefits of such an approach have been demonstrated for an SMB where supercritical carbon dioxide is used as a solvent. In this case in fact, the operating pressure and density have a significant effect on retention, and by applying a pressure gradient (with the pressure decreasing from section 1 to section 4) productivity can be significantly improved with respect to the constant pressure operation. This has been demonstrated both experimentally [5,6], and theoretically [7,8], and represents a very promising concept with potential for concrete applications. Another possibility is that of operating sections 1 and 2 at a higher temperature than sections 3 and 4; the advantages and limitations of this approach have been recently investigated theoretically [9], but no temperature gradient SMB has been experimentally tested so far.

Gradient elution chromatography is widely used for analytical purposes, and exploits the effect of mobile phase composition on the retention behavior of solutes. Applying this concept to the SMB technology, thus operating SMBs in the solvent gradient mode, is the subject of this work and of other recent contributions in the literature [10,11]. The typical solvent gradient implementation involves the use of two solvents with different properties, e.g. a more and a less polar one, and the tuning of their relative composition along the SMB unit.

Our objective is to derive design criteria for binary SMB separations operated in the solvent gradient

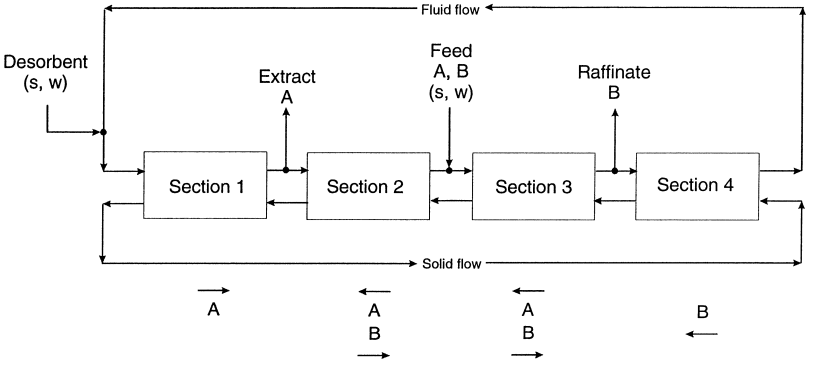

Fig. 1. Scheme of a closed loop true moving bed unit.

mode, where for the sake of simplicity the concentration of the solutes is low enough that their adsorption isotherms are linear:

$$q_i = H_i c_i \quad (i = A,B), \tag{1}$$

where c_i and q_i are the fluid and adsorbed phase concentrations, respectively, and H_i is the Henry's constant. Allowing for solvent composition changes along the SMB unit increases the number of degrees of freedom, thus making the overall optimization of the separation a more complex problem. In addition to the adsorption equilibria, several other physical properties such as viscosity, density, and solubility depend on the mobile phase composition. These have an important impact on SMB operation and optimization, through their effect on pressure drop, column efficiency, and maximum allowable feed concentration of the species to be separated. As a consequence, optimizing solvent gradient SMBs requires a fairly large amount of physico–chemical data. However, knowing the complete separation region in terms of fluid flow-rates and switch time as a function of the solvent composition profile in the SMB is a prerequisite to tackle and master the overall optimization problem. Therefore, it is the objective of this work to determine the complete separation region in the operating parameter space, and to clarify the features of solvent gradient operation, without actually attempting to identify optimal operating conditions, e.g. optimal solvent gradient profile and optimal operating point.

2. Retention behavior in mixed solvents

It is well known in analytical chromatography that changing the mobile phase composition, e.g. either changing the ratio between a polar and an apolar solvent, or changing the pH of the solution, modifies significantly the retention behavior of the solutes. For example, the effect of increasing the water content in a water–methanol mixture on the Henry's constants of the enantiomers of α-ionone on a Nucleodex-β-PM, Macherey–Nagel, Düren, Germany, 30 × 4 mm, stationary phase: heptakis(2,3,6-per-*O*-methyl)-*β*-cyclodextrin bonded to silica gel; particle diameter: 5 μm) is illustrated in Fig. 2.

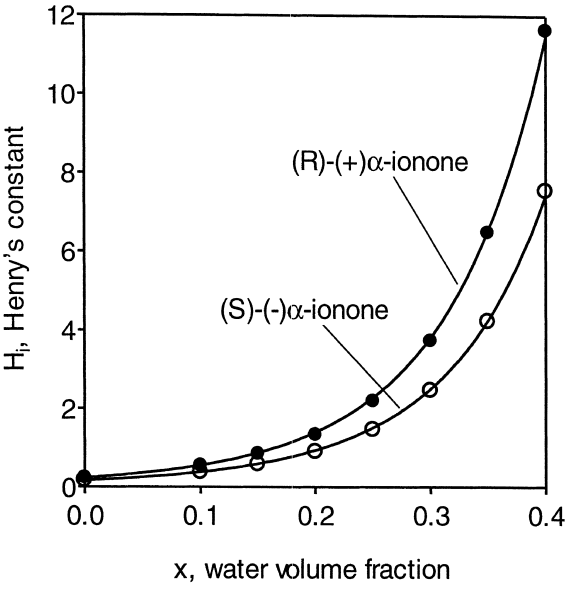

Fig. 2. Enantiomers of α-ionone in methanol–water mobile phases. Henry's constants as a function of the water volume fraction, *x*. Symbols are the measured values, whereas solid lines are calculated using Eq. (2) and the following dimensionless parameter values: $H_A^0 = 0.24$, $H_B^0 = 0.17$, $k_A = 0.75$, $k_B = 0.80$, $n_A = 10.85$, and $n_B = 9.80$.

It is rather clear that changing the mobile phase composition modifies at the same time the affinity of the solutes for the fluid phase, i.e. their solubility, as well as their adsorptivity on the stationary phase. The latter effect may be due either to modifications of the distribution of the surface charges in the different fluid environments, or to true competitive adsorption of one or both solvents on the stationary phase itself. Most likely, both phenomena are present to a certain extent. However, in the following we will be content to describe data such as those in Fig. 2, in an empiric way, namely using the following non-linear interpolating function:

$$H_i = H_i(x) = \frac{H_i^0}{(1 - k_i x)^{n_i}} \quad (i = A,B), \tag{2}$$

where *x* represents the fraction (normally, a volume fraction) of the solvent (indicated in the following as solvent W), with elution strength smaller than the other (indicated in the following as solvent S); H_i^0 is

the Henry's constant at $x = 0$, i.e. where only solvent S is used; k_i and n_i are positive parameters describing the effect of x on retention. Since selectivity is given by the ratio H_A/H_B, it is also a function of mobile phase composition unless $k_A = k_B$ and $n_A = n_B$. The data in Fig. 2, where x represents the water volume fraction are well described using the parameter values (all dimensionless): $H_A^0 = 0.24$, $H^0{}_B = 0.17$, $k_A = 0.75$, $k_B = 0.80$, $n_A = 10.85$, and $n_B = 9.80$. In this case selectivity is 1.41 in pure methanol, and increases to 1.54 in a solution with 40% volume of water.

3. Solvent gradient simulated moving bed (SG-SMB)

Let us refer to the closed-loop configuration shown in Fig. 1, where the outlet stream from section 4 is recycled to section 1 after mixing with the desorbent stream. A composition profile for the mobile phase can be established in a simple way by feeding two different mobile phase compositions through the desorbent and feed ports. Let us indicate the volume fraction of the weak solvent W in the desorbent and in the feed with the symbols, x_D and x_F, respectively. Within the unit the mobile phase composition will be intermediate between the two inlet compositions. In particular, if $x_D < x_F$, i.e. the desorbent is reacher than the feed in the solvent with the greater elution strength, then retention times will be smaller in sections 1 and 2 than in sections 3 and 4.

This situation is illustrated in Fig. 3 for a TMB; the mobile phase composition profiles in each section are flat at steady state, in a TMB unit where axial dispersion is neglected. In the following we identify the solvent W fraction in sections 1 and 2 as x_2, and that in sections 3 and 4 as x_3. These values for given inlet compositions $x_D < x_F$ depend on the external and internal flow-rates, and are calculated through the balances for solvent W at the desorbent and the feed nodes:

$$x_F Q_F + x_2 Q_2^{TMB} = x_3 Q_3^{TMB} \tag{3}$$

$$x_3 Q_4^{TMB} + x_D Q_D = x_2 Q_1^{TMB}, \tag{4}$$

where Q represents volume flow-rates, and for the sake of simplicity volume changes upon mixing have been neglected. The inequalities $x_D \leq x_2 \leq x_3 \leq x_F$ follow from these equations.

In a SG-SMB the composition profile is less regular, due to the non-steady state nature of its behavior, and the profile drawn in Fig. 3 represents only an idealization of the real profile. The latter depends on the operating conditions; it can be pretty close to the TMB one, but also rather different. An example of such a profile is illustrated in Fig. 4; this has been calculated using a standard lumped solid diffusion model of the SG-SMB [12]. The operating conditions reported in the caption of the figure were designed to attain $x_2 = 0.34$ and $x_3 = 0.45$; the

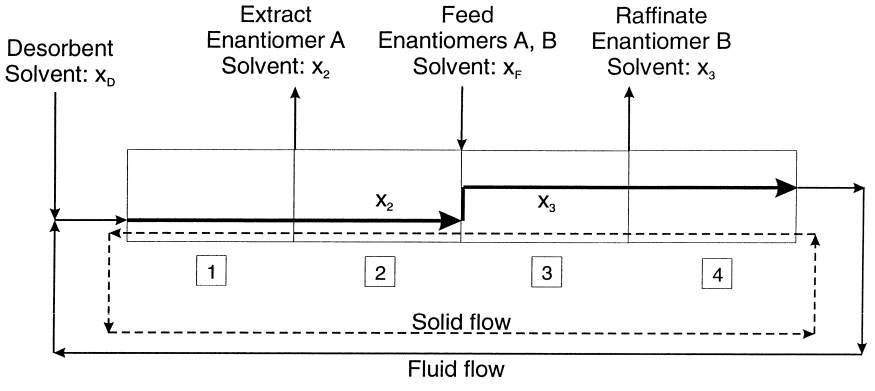

Fig. 3. Mobile phase composition profile in a SG-TMB unit where the external mobile phase compositions are x_D and x_F, with $x_D \leq x_2 \leq x_3 \leq x_F$.

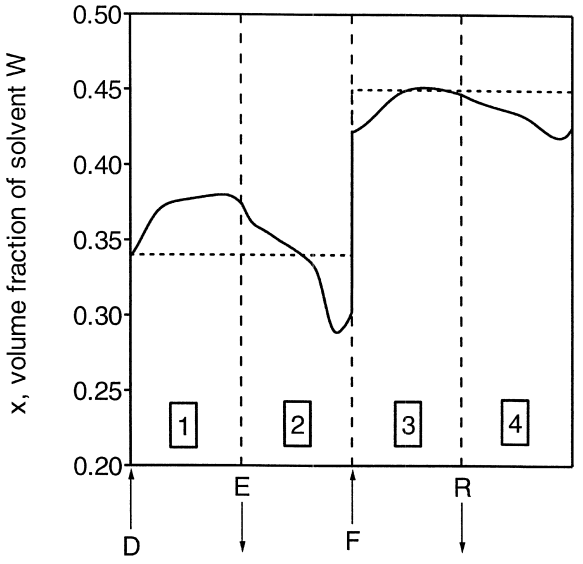

Fig. 4. Comparison between the mobile phase composition profile in a SG-TMB (broken line) and in the equivalent SG-SMB with a 2-2-2-2 configuration (solid line). In the latter case, the profile is calculated for cyclic steady state conditions, and plotted at the end of the period between two port switches, just before the next port switch.

profile corresponds to a point in time at the end of a time period between two port switches, immediately before the switch. It is worth noting that the desired x_2 and x_3 values are shown by the horizontal broken lines in the figure, and that these correspond to the space and time average of the actual concentration profiles attained in sections 1 and 2, and 3 and 4, respectively. The difference between the profiles in Figs. 3 and 4 stems from the intrinsic difference between the counter-current TMB process and the simulated counter-current SMB process.

It is worth noting that the analysis that follows applies also to the case of an SMB operated in an open-loop configuration, i.e. without direct recycle of the stream coming out of section 4. Since the stream entering section 1 is just the desorbent stream, then in this case $x_2 = x_D$, and Eq. (4) does not apply.

The above discussion clarifies similarities and differences between TMB and SMB behavior in the solvent gradient operation mode. Despite these differences, it is convenient to use the TMB model to identify feasible operating regions in the operating parameter space at least as a first approximation, and then to translate these into flow-rates and switch time of the equivalent SMB unit. A direct analysis of the SMB unit with the usual detailed models can be performed afterwards as a refinement step. This approach will be followed in our analysis. SMB and TMB units are considered to be equivalent and to achieve in principle the same separation performance provided geometric and kinematic conversion rules given by the following relationships are fulfilled [1,13]:

$$\frac{V}{t^*} = \frac{Q_s}{1-\varepsilon_b} \tag{5}$$

$$Q_j^{SMB} = \left[Q_j^{TMB} + \frac{Q_s \varepsilon_b}{1-\varepsilon_b} \right], \tag{6}$$

where Q_j^{SMB}, Q_j^{TMB}, and Q_s are the fluid and the solid flow-rate, respectively; V is the column volume; ε_b and ε_p are bed void fraction and particle porosity, respectively; t^* is the switch time in the SMB unit. Operating conditions will be conveniently given in terms of the flow-rate ratios, m_j, $j = 1, \ldots, 4$, defined as follows [14]:

$$m_j = \frac{Q_j^{SMB} t^* - V\varepsilon^*}{V(1-\varepsilon^*)} = \frac{Q_j^{TMB} - Q_s \varepsilon_p}{Q_s(1-\varepsilon_p)}, \tag{7}$$

where $\varepsilon^* = \varepsilon_b + (1-\varepsilon_b)\varepsilon_p$ is the overall bed void fraction.

4. Operating conditions for complete separation

With reference to the SG-TMB unit in Fig. 1, the following conditions on the flow-rate ratios are necessary and sufficient to achieve complete separation in the case where adsorption isotherms are linear, i.e. $q_i = H_i(x)c_i$ [1,13]:

$$H_A(x_2) < m_1 \tag{8}$$

$$H_B(x_2) < m_2 < H_A(x_2) \tag{9}$$

$$H_B(x_3) < m_3 < H_A(x_3) \tag{10}$$

$$m_4 < H_B(x_3). \tag{11}$$

Since Henry's constants depend upon the mobile phase composition through the parameter x, the

lower and upper bounds of the m_j values to be adopted depend on the mobile phase composition as well. The parameters x_2 and x_3 can be calculated through the solvent balances (3) and (4), which can be recast in terms of flow-rate ratios and accounting for overall material balances at the feed and the desorbent nodes as follows:

$$m_3(x_F - x_3) = m_2(x_F - x_2) \quad (12)$$

$$m_1(x_2 - x_D) = m_4(x_3 - x_D). \quad (13)$$

Note that these two equations apply also in the case of porous particles, i.e. $\varepsilon_p > 0$, since the solvents are considered non-adsorbable.

Solving Eqs. (12) and (13) for x_2 and x_3 in terms of x_D, x_F, and the flow-rate ratios, and substituting the resulting expressions in Eqs. (8) to (11) yields a set of inequalities in the four unknowns m_j ($j = 1, \ldots, 4$). This is a non-linear system due to the non-linear dependence of H_i on x through Eq. (2), which defines a region in the four dimensional space spanned by the four flow-rate ratios. In the frame of equilibrium theory the points belonging to this region allow achieving complete separation of species A and B, i.e. pure A in the extract and pure B in the raffinate. The boundaries of this region depends only on the external mobile phase compositions x_D and x_F, and on the retention behavior of the solutes, which is described by Eq. (2).

In order to apply this result to the design of the separation in the gradient mode, it is worth developing a geometrical representation of the complete separation region [14]. This can be done rather effectively following a step by step approach, which can be easily extended also to the case of non-linear isotherms, and is presented in the next section.

5. The region of complete separation

In this section we consider the separation problem for fixed mobile phase composition in the desorbent, x_D, and in the feed, x_F. The objective is to define operating conditions in terms of flow-rate ratios m_j, i.e. in terms of fluid and solid flow-rates in the TMB unit (and in terms of fluid flow-rates and switch time for the corresponding SMB unit) that lead to complete separation. The procedure to determine the complete separation region is outlined in various steps in the following. With illustrative purposes, as a model system a mixture of two components A and B is considered; the relative composition of the two species need not be specified since adsorption follows the linear isotherm (1). The corresponding parameters in Eq. (2) are $H_A^0 = 2.12$, $H^0{}_B = 1.41$, $k_A = k_B = 0.95$, and $n_A = n_B = 1$. The complete separation region will be calculated for $x_D = 0$ and $x_F = 0.9$.

5.1. Complete separation region for a fixed pair (x_2, x_3)

When the values of x_2 and x_3 are fixed, the upper and lower bounds in Eqs. (8) to (11) are known and independent from the flow-rate ratios. The projection of the corresponding complete separation region onto the (m_2, m_3) plane is a rectangle, of which only the portion above the diagonal, i.e. where $m_3 > m_2$, allows having a positive feed flow-rate. The case where $x_2 = 0.2$ and $x_3 = 0.6$ is illustrated in Fig. 5; we will call this *the complete separation region for the given* (x_2, x_3) *pair*. It is worth considering all the regions drawn in the figure beside the complete separation rectangle 1. In region 2 the raffinate is polluted with component A, in region 3 the extract is polluted with component B, and in region 4 both extract and raffinate contain both A and B. In regions 5 and 6 both A and B exit the unit entirely in the raffinate or entirely in the extract, respectively. Regions 7, 8, and 9 are not feasible since in the frame of a linear adsorption analysis either component A (in region 7), or component B (in region 8), or both (in region 9), cannot leave the unit and therefore accumulate indefinitely. In reality, their hold-up is upper bounded by the achievement of saturation conditions either in the fluid or in the adsorbed phase. In this case the linear description is no more valid, and must be replaced by a non-linear analysis.

However, in the SG-TMB the four m_j values must fulfill also the solvent balances Eqs. (12) and (13); this reduces the number of degrees of freedom from four to two only. In particular, the operating point in the (m_2, m_3) plane must belong to the operating line defined by Eq. (12). With reference to Fig. 5, only the points belonging to the segment along the

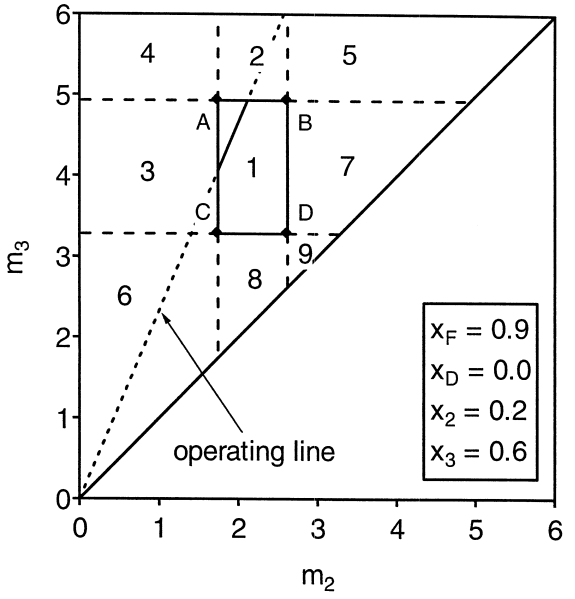

Fig. 5. Complete separation region in the (m_2, m_3) plane for a fixed pair (x_2, x_3), and operating line given by Eq. (12) for the solvent gradient mode operation. The regions are calculated for the model system with the following retention parameters: $H_A^0 = 2.12$, $H_B^0 = 1.41$, $k_A = k_B = 0.95$, and $n_A = n_B = 1$. Mobile phase composition values are reported in the box. Classification: region 1, complete separation; 2, pure extract and raffinate polluted with component A; 3, pure raffinate and extract polluted with component B; 4, both extract and raffinate containing both A and B; 5, extract flooded with pure desorbent, both A and B entirely collected in the raffinate; 6, raffinate flooded with pure desorbent, both A and B entirely collected in the extract; 7, extract flooded with pure desorbent, pure raffinate, and A accumulating in the unit; 8, raffinate flooded with pure desorbent, pure extract, and B accumulating in the unit; 9, both raffinate and extract flooded with pure desorbent, both A and B accumulating in the unit.

operating line (12) that intersects the rectangle are compatible with the mobile phase compositions x_2 and x_3, and allow achieving complete separation.

At the same time the flow-rate ratios m_1 and m_4 must be one proportional to the other according to Eq. (13) and fulfill inequalities (8) and (11). The following inequality, which is derived by combining the three equations just mentioned, guarantees that there exists a finite range of feasible values of m_4 (and hence of m_1):

$$(x_3 - x_D)H_B(x_3) \geq (x_2 - x_D)H_A(x_2) \ . \qquad (14)$$

This is actually a constraint on the pair (x_2, x_3); only combinations of mobile phase composition levels that fulfill the last inequality allow for the achievement of regeneration of the solid-phase in section 1 and of the mobile phase in section 4. Eq. (14) implies that x_3 must be strictly larger than x_2; how much larger depends on the specific functional form of $H_A(x)$ and $H_B(x)$. It is worth noting however, that if the unit is operated in the open-loop configuration, then Eqs. (13) and (14) do not apply. In this case, x_3 can be equal to x_2, which according to Eq. (12) occurs only on the diagonal of the (m_2, m_3) plane where $Q_F = 0$.

5.2. Complete separation region for a fixed value of x_2

Let us now vary x_3, while keeping x_2 constant. The effect of increasing x_3 when $x_2 = 0.2$ is illustrated in Fig. 6; four different intersecting segments corresponding to $x_3 = 0.4$, 0.5, 0.6, 0.7, are highlighted. It is rather clear that when further increasing x_3, a value is eventually reached where the operating

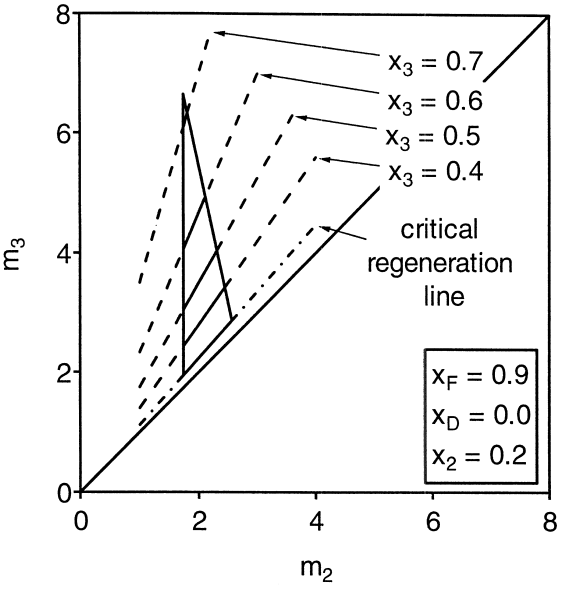

Fig. 6. Operating lines for constant $x_2 = 0.2$, and $x_3 = 0.4$, 0.5, 0.6, 0.7, for the model system. The solid parts, but not the dashed parts, of the operating lines belong to the complete separation region for $x_2 = 0.2$; this is obtained by combining all the solid segments. The dashed-dotted line represents the critical regeneration line.

line and the corresponding rectangle do not intersect any more; this occurrance indicates that the selected pair (x_2, x_3) does not allow for complete separation. These considerations show that there exists a maximum x_3 value, which is defined as that where the intersection between operating line and rectangle in the (m_2, m_3) plane reduces to a point,

Thus summarizing, for a fixed value of x_2 there is a minimum value of x_3 defined by Eq. (14) which guarantees proper operation of sections 1 and 4 and a maximum x_3 value beyond which sections 2 and 3 do not separate components A and B any more. Thus, *the complete separation region for the given* x_2 *value* in the (m_2, m_3) plane is obtained by putting together the intersecting segments for all the feasible x_3 values. This is illustrated in Fig. 6 for the model system, where the obtained region has a triangular shape, and its basis is the critical regeneration line, i.e. the operating line corresponding to the minimum x_3 value.

The complete separation region for $x_2 = 0.5$ is drawn in Fig. 7, together with the regions where a different regime is attained; this is identified by a number, with a meaning identical to that used in Fig. 5. It is worth noting that in this particular case the unfeasible regions 7, 8, and 9 are missing, whereas the region R below the critical regeneration line is present. The boundaries of region 1 (solid lines), and the boundaries between the other regions (broken lines) in Fig. 7, as well as in Fig. 9 discussed in Section 5.4 below, are given by the following relationships. These are obtained by tracking the intersections between the operating line (12) and all the region boundaries shown in Fig. 5, as x_3 is varied at constant x_2. In addition, the straight line that constitutes the upper boundary of region R is obtained using Eq. (13) and the minimum m_3 value obtained by solving Eq. (14).

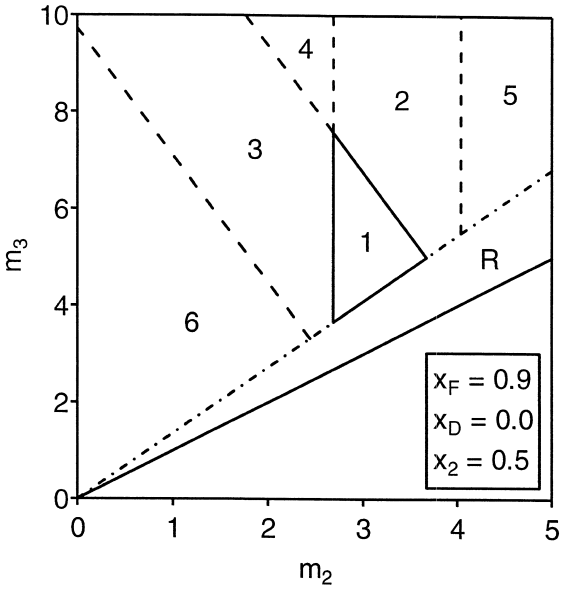

Fig. 7. Complete separation region for $x_2 = 0.5$ for the model system with $x_F = 0.9$, and $x_D = 0.0$. The same classification of the regions as in Fig. 5 applies. The region R is below the critical regeneration, hence extract and raffinate are polluted due to incomplete regeneration in sections 1 and 4.

- Vertical line separating regions 2–5, 1–7, and 8–9:

$$m_2 = H_A(x_2). \tag{15}$$

- Vertical line separating regions 1–3, 2–4, and 6–8:

$$m_2 = H_B(x_2). \tag{16}$$

- Curve separating regions 1–2, 3–4, and 5–7:

$$m_2 = \frac{m_3^{\frac{n_A-1}{n_A}}}{k_A(x_F - x_2)}\left[m_3^{\frac{1}{n_A}}(k_A x_F - 1) + (H_A{}^0)^{\frac{1}{n_A}} \right]. \tag{17}$$

- Curve separating regions 1–8, 3–6, and 7–9:

$$m_2 = \frac{m_3^{\frac{n_B-1}{n_B}}}{k_B(x_F - x_2)}\left[m_3^{\frac{1}{n_B}}(k_B x_F - 1) + (H_B{}^0)^{\frac{1}{n_B}} \right]. \tag{18}$$

When $n_i = 1$ for either $i = A$ or $i = B$ as in the case of the model system, then a straight line is obtained using either Eqs. (17) or (18), respectively.

5.3. Complete separation region

Let us now vary x_2 as well. As illustrated in Fig. 8, the complete separation regions for each individual x_2 value move to the upper right corner of the diagram and shrink while x_2 increases. It is found

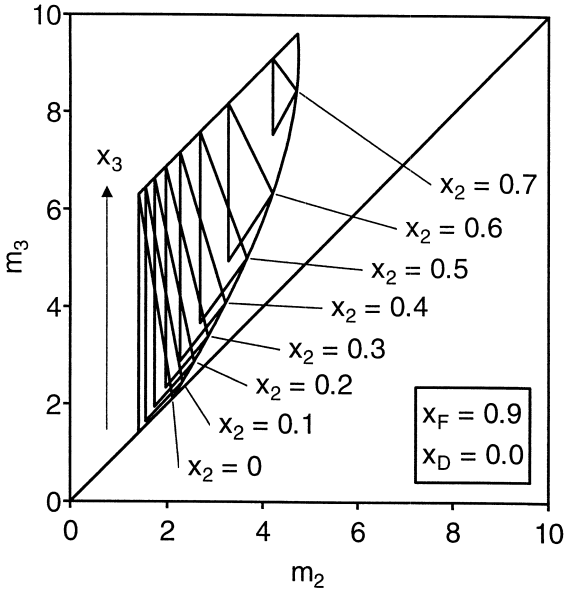

Fig. 8. Complete separation regions for different values of x_2 for the model system with $x_F = 0.9$, and $x_D = 0.0$. The complete separation region for the given pair (x_D, x_F) is obtained by combining all these. The leftmost region, whose basis is on the diagonal, applies to the open-loop unit where $x_2 = x_D$.

that when further increasing x_2, a maximum value is eventually achieved where there are no more feasible operating points. On the other hand, x_2 cannot be smaller than x_D. Where $x_2 = x_D$, either $m_4 = 0$ to fulfill Eq. (13) or the SG-SMB unit is operated in the open-loop configuration; in both cases, the corresponding critical regeneration line coincides with the diagonal. Thus, *the complete separation region* is finally obtained by putting together all the complete separation regions for the x_2 values between the minimum and the maximum ones. This depends only on the mobile phase composition in the external streams, i.e. on x_D and x_F; as a matter of fact Fig. 8 provides a geometrical representation of the solution of the mathematical problem stated in section 4. It is worth underlying that for the operating points in the complete separation region all flow-rates, both external and internal, may be different, whereas only x_D and x_F are constant.

5.4. Effect of retention model parameters

In this section the effect of the parameters describing the retention behavior of the solutes as a function of the mobile phase composition, i.e. those in Eq. (2), is considered. When applying Eq. (15) to (18) to systems with n_i values larger or smaller than 1 and with k_i values different from each other, the shape of the complete separation region for a fixed x_2 value can be rather different from that obtained for the model system and shown in Fig. 6. Two examples for two different values of x_F are given in Fig. 9, which applies to the α-ionone system whose retention behavior is illustrated in Fig. 2. It can be readily observed that all types of separation regime discussed with reference to Fig. 5 can be observed also in this case, i.e. regions 1 to 9. Moreover, the interaction between solvent balances and separation conditions may be such that the complete separation region for a fixed x_2 value may be constituted of two disjoint parts, as in Fig. 9b.

Also when considering the complete separation region the effect of the retention model parameters is rather significant. This is illustrated in Fig. 10 where four different cases are considered. It is worth noting that the complete separation region can be either convex as in Fig. 10a and d, or concave as in Fig. 10b and c. Moreover, the curve that constitutes the upper boundary of the complete separation region is given by the following equation, which is obtained by interesecting curves (16) and (17):

$$k_B m_3^{\frac{n_A-1}{n_A}}\left[m_3^{\frac{1}{n_A}}(k_A x_F - 1) + (H_A^0)^{\frac{1}{n_A}}\right] = k_A m_2^{\frac{n_B-1}{n_B}}\left[m_2^{\frac{1}{n_B}}(k_B x_F - 1) + (H_B^0)^{\frac{1}{n_B}}\right]. \quad (19)$$

This represents a straight line only where $n_A = n_B = 1$, i.e. in the cases illustrated in Figs. 8, 10a and b.

5.5. Effect of mobile phase composition

In this section the role of the mobile phase composition of the external streams, i.e. x_D and x_F, on the shape and position of the complete separation region is analyzed. This is of course worth investigating, since these two parameters are of key importance for the overall optimization of the SG-SMB separation. Here, we consider the effect of mobile phase composition on the retention behavior of the two components to be separated only, while

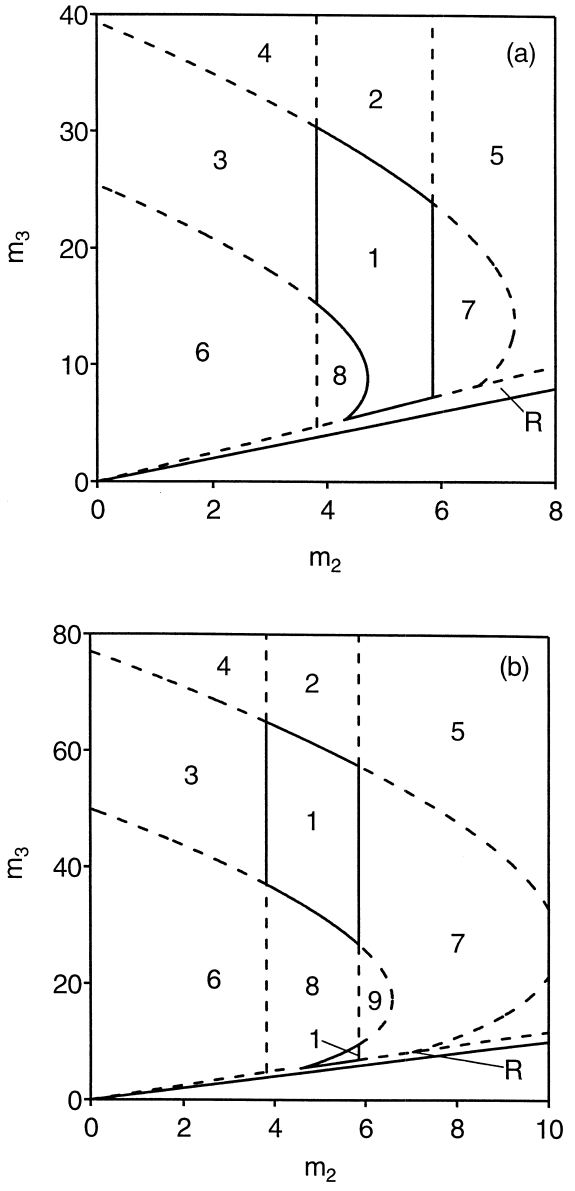

Fig. 9. Complete separation regions for a given x_2 value for the system α-ionone in water/methanol with: (a) $x_2 = 0.34$, $x_F = 0.5$ and $x_D = 0.0$; (b) $x_2 = 0.34$, $x_F = 0.55$ and $x_D = 0.0$. The same classification of the regions as in Fig. 7 applies.

neglecting any effect on solubility, density, and viscosity. As a consequence, the whole range of mobile phase composition from pure S solvent to pure W solvent is considered, even though in most real cases only a limited range of composition is practically accessible. Sometimes, for instance, the stationary phase itself is stable only below a certain relative concentration of one of the two solvents, hence this upper limit cannot be overcome in practice.

With reference to the model system, whose complete separation region for $x_D = 0$ and $x_F = 0.9$ is shown in Fig. 8, the effect of changing the mobile phase composition in the feed x_F at constant $x_D = 0$ is illustrated in Fig. 11a, whereas the effect of changing that in the desorbent stream at constant $x_F = 1$ is shown in Fig. 11b. It can be observed that in the former case (Fig. 11a) the complete separation region becomes larger as x_F increases. The largest region is obtained when pure solvent S is fed as desorbent, and pure solvent W is fed with the feed. However, it is worth noting that these are precisely the conditions that are typically difficult to apply in practice for the reasons mentioned above. In the latter case on the contrary (Fig. 11b), the complete separation region shifts along the diagonal towards the upper right corner of the diagram as x_D increases without significantly changing its size; of course when x_D becomes equal to x_F the complete separation region reduces to the well known linear triangle for isocratic operation. Although, the change of the complete separation region with the composition of the feed and desorbent streams is affected by the values of the retention model parameters, the trends observed are quite general.

6. SG-SMB design and operation

In this section we discuss how an existing SG-SMB can be operated to achieve the desired separation performance, i.e complete separation of the two solutes A and B. In the following we assume that the external mobile phase composition is fixed, i.e. that x_D and x_F have already been selected. In this context, we can assume that this choice is based on considerations, which do not depend only on the retention behavior of the two solutes, but also on the other properties such as solubility, viscosity, and density. In general, it can be said that the maximum possible difference between x_F and x_D should be

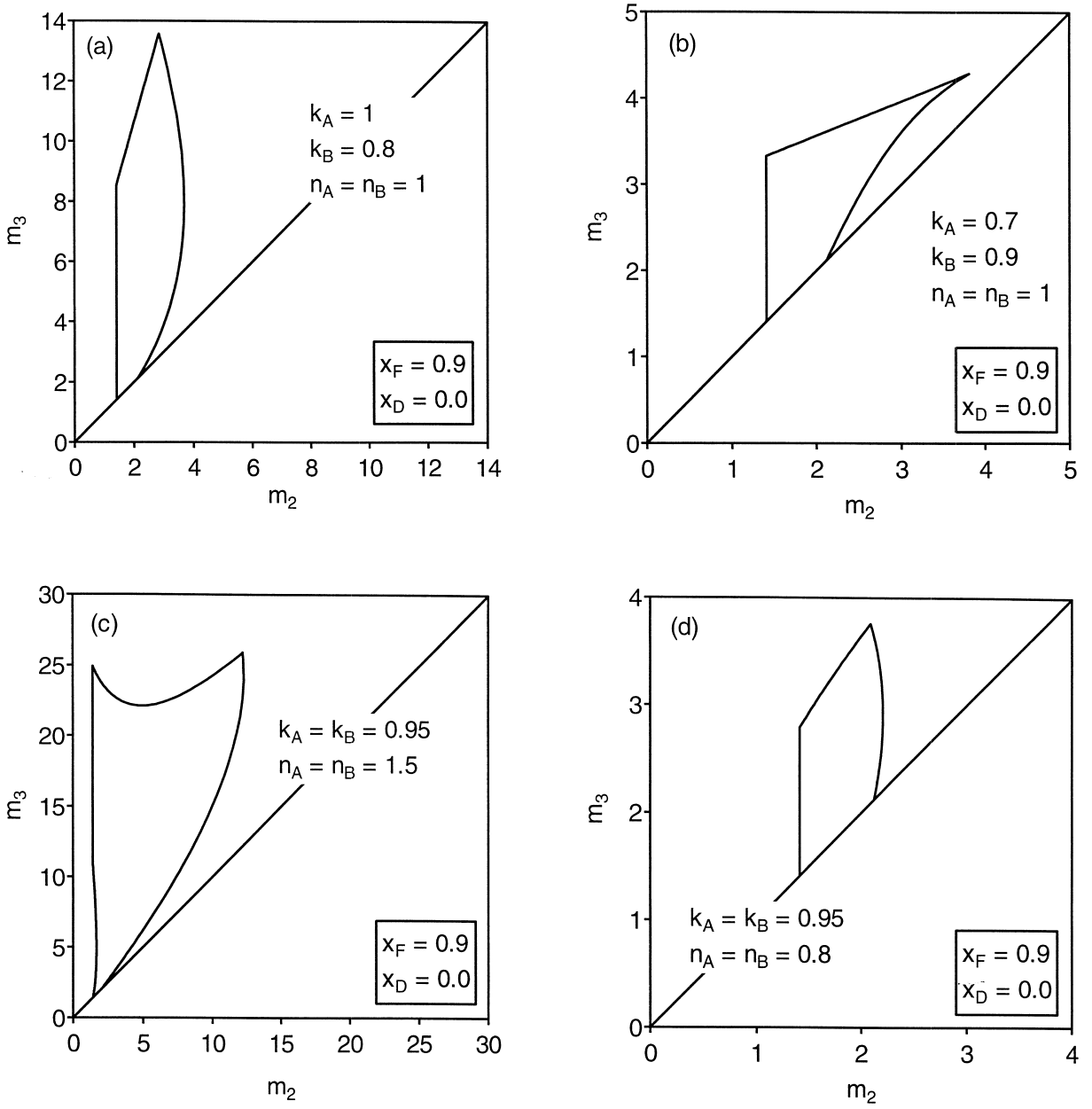

Fig. 10. Complete separation regions for different systems with $x_F = 0.9$ and $x_D = 0.0$. Retention parameters: $H_A^0 = 2.12$, $H_B^0 = 1.41$; (a) $k_A = 1$, $k_B = 0.8$, $n_A = n_B = 1$; (b) $k_A = 0.7$, $k_B = 0.9$, $n_A = n_B = 1$; (c) $k_A = k_B = 0.95$, $n_A = n_B = 1.5$; (d) $k_A = k_B = 0.95$, $n_A = n_B = 0.8$.

adopted. To illustrate the discussion, the model system introduced in section 5 will be considered once more.

6.1. Choosing an operating point

Choosing an operating point for an SG-SMB

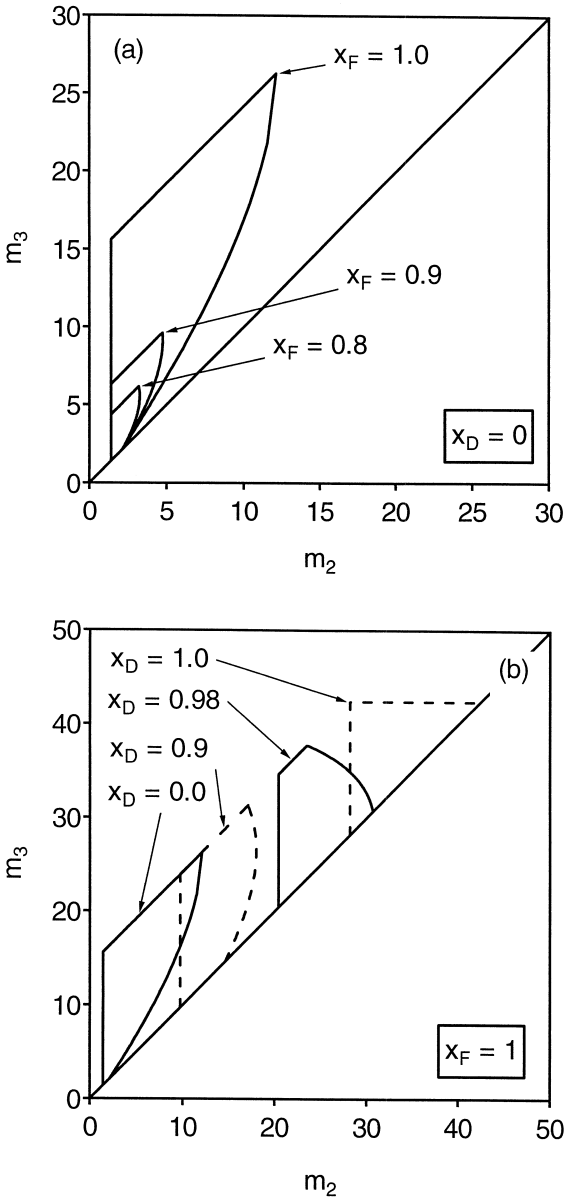

Fig. 11. Complete separation regions for the model system for different external mobile phase compositions. (a) Effect of changing x_F at constant $x_D = 0$. (b) Effect of changing x_D at constant $x_F = 1$.

separation with a given pair of values x_D and x_F requires that all internal flow-rates, Q_j, $j = 1, \ldots, 4$, and the switch time are selected. In the operating parameter space, an operating point that allows achieving complete separation must belong to the

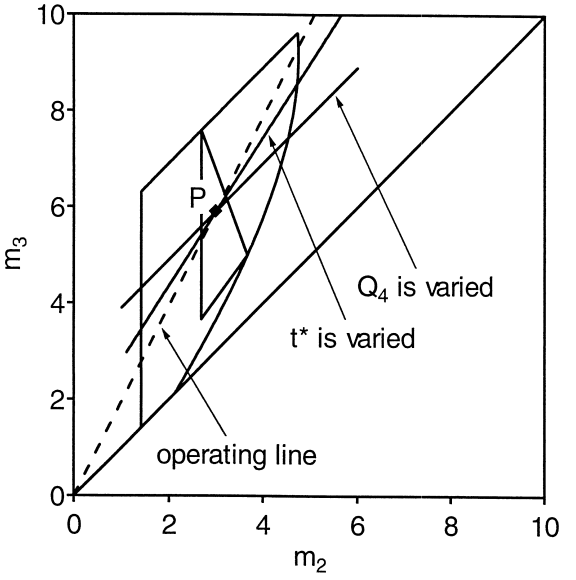

Fig. 12. Design and operation of a SG-SMB unit, in the case of the model system with $x_F = 0.9$, and $x_D = 0.0$. Operating point P within the complete separation region for $x_2 = 0.5$. The dashed line is the operating line of Eq. (12), whereas the two solid lines are given by Eqs. (20) and (21).

corresponding complete separation region drawn in Fig. 12; in this particular case $x_D = 0$, and $x_F = 0.9$. For each point in such a region a suitable combination of m_j ($j = 1, \ldots, 4$) values can be found that fulfills the solvent mass balances (12) and (13), and the constraints to achieve complete separation (8) to (11). The exact location of the point is chosen based on performance and robustness considerations [13,14]. These will involve an evaluation about the productivity, the solvent consumption, and the robustness of the separation, which means that small disturbances do not significantly modify the separation performance of the unit. These aspects would define which specific point in the complete separation region leads to the best performance. As discussed above, we do not consider this issue here, which most likely would also depend on the specificity of the particular separation under consideration, and simply select one point within the complete separation region, say point P in Fig. 12, and develop further the SG-SMB design procedure. Note that the selected point is rather far from the boundaries, so as to guarantee that all the non-ideal effects, which are neglected in the theoretical analysis based on the

equilibrium theory analysis of the equivalent SG-TMB configuration, are not going to hinder the separation performance significantly. The choice of P assigns the values of m_2 and m_3.

By considering again Fig. 8, it is observed that the chosen point P belongs to a whole set of complete separation regions for given values of x_2 in a well defined range. In principle any x_2 value among these can be selected; in practice, x_2 is chosen in such a way that P is located in a balanced position within the corresponding complete separation region, as illustrated in Fig. 12. In other words, the complete separation region for the selected x_2 value should be such that P is not too close to any of its boundaries.

Given m_2,m_3 and x_2, the solvent balance (12) is solved for x_3, and then the ratio m_1/m_4 is calculated through the second solvent balance (13). Since point P is in the complete separation region, i.e. above the critical regeneration line, there is certainly a range of values of m_1 and m_4, which fulfill Eq. (13), as well as the constraints (8) and (11). Values of these two parameters within this range are chosen in order to keep both of them at the largest possible distance from the corresponding lower and upper bounds given by Eqs. (8) and (11).

Finally, a value for t^* is chosen based on usual pressure drop and efficiency considerations [15]. Once t^* is selected, for every section the internal flow-rate Q_j is calculated using the known value of m_j and Eq. (7). From the overall material balances at the inlet and outlet nodes of the unit the external flow-rates are eventually calculated.

6.2. Tuning the separation performance

When running experiments on an SMB unit in a given operating point, e.g. P of coordinates (m_2^P,m_3^P) in Fig. 12, there is often the need to adjust the operating conditions either to improve the separation performance or to analyse significant effects. If only a fine tuning is required, the operating point is moved in such a way to minimize the number of operating parameters to be actually changed. In practice this is done by changing only either the switch time t^* or the recycle flow-rate Q_4 in closed-loop SMBs (the desorbent flow-rate Q_1 in open loop SMBs). In the former case all internal and external flow-rates are left unchanged, but all flow-rate ratios m_j change linearly with t^*. In the latter case, the switch time and all external flow-rates are constant, but the internal flow-rates increase or decrease following Q_4, and so do also the m_j values according to Eq. (7).

It is rather straightforward to show that following one or the other of the two experimental strategies above, the new operating point belongs to two different straight lines intersecting in point P (see Fig. 12). The following are the corresponding equations:

$$m_3 = \frac{Q_3}{Q_2}\, m_2 + \left[m_3^P - m_2^P\, \frac{Q_3}{Q_2} \right], \tag{20}$$

$$m_3 = m_2 + m_3^P - m_2^P, \tag{21}$$

which apply to the changes in switch time and in recycle flow-rate, respectively. It is worth noting that in Eq. (20) the symbols Q_2 and Q_3 are not ambiguous, since these two parameters remain constant along the corresponding straight line. Increasing either t^* or Q_4 moves the operating point along the corresponding line towards larger values of m_2 and m_3.

It can be readily observed that neither straight line coincides with the operating line given by Eq. (12), along which the internal mobile phase composition levels x_2 and x_3, that are calculated for the equivalent SG-TMB unit and represent average values of the actual mobile phase composition profile in the SG-SMB unit, remain constant. The new x_2 and x_3 are in fact given by solving Eqs. (12) and (13) for the new set of m_j values. Therefore, both the above mentioned strategies yield changes in the values of x_2 and x_3. Thus, the position of the new operating point should be evaluated with respect to the complete separation region for the new x_2 value and not with respect to the one drawn in Fig. 12. In principle, this makes things more complicated than in the isocratic case. In practice, the key trends observed in the isocratic case are observed also in the solvent gradient case, and can be summarized as follows. When increasing either t^* or Q_4, the operating point moves towards the region where the raffinate gets polluted with component A, and accordingly raffinate purity decreases and extract purity increases if it is not already 100%. On the contrary, when decreasing either t^* or Q_4, the operating point moves

towards the region where the extract gets polluted with component B, and accordingly extract purity decreases and raffinate purity increases, if not already 100%. In other words, increasing either parameter moves the concentration fronts towards the raffinate outlet, whereas the opposite occurs when either t^* or Q_4 decreases.

7. Discussion and conclusions

The conclusions drawn through the theoretical analysis developed above are based on an ideal description of the SG-SMB process, where a number of important assumptions have been made. First, non-ideal effects, i.e. axial dispersion and mass transfer resistance, are neglected in the description of the column dynamics. The equilibrium theory model is in fact adopted. Secondly, it is assumed that the separation performance of the SG-TMB unit is the same as that of the SG-SMB, which is equivalent to it according to the definition embedded in Eqs. (5) and (6); this is assumed despite the evident differences exhibited by the mobile phase composition profiles in the two unit configurations, as illustrated in Fig. 4. Finally, the complex interaction among the two solutes, the two solvents, and the stationary phase is described through the linear adsorption isotherm (1), where the Henry's constants depend on the mobile phase composition through Eq. (2).

Whereas the third assumption can be verified only through experiments and represents anyhow a realistic possibility in chromatography, the first two can be easily verified through numerical simulations of the SG-SMB behavior. Thus, simulations have been carried out using a detailed description of the SMB process, which is based on the lumped solid diffusion model to describe each individual chromatographic column [12]. Thus, the column model is constituted of two material balance equations for each component A and B, and of a balance equation for the weak solvent W. The former are written in terms of molar concentrations, whereas the latter in terms of volume fraction, under the assumption of negligible volume effects upon mixing:

$$\varepsilon^* \frac{\partial c_i}{\partial t} + (1-\varepsilon^*)\frac{\partial q_i}{\partial t} + u\frac{\partial c_i}{\partial z} = \varepsilon_b D_i \frac{\partial^2 c_i}{\partial z^2} \quad (i = A,B) \tag{22}$$

$$\frac{\partial q_i}{\partial t} = k_{q,i} a_p \, [H_i(x) c_i - q_i] \quad (i = A,B) \tag{23}$$

$$\varepsilon^* \frac{\partial x}{\partial t} + u\frac{\partial x}{\partial z} = \varepsilon_b D_W \frac{\partial^2 x}{\partial z^2} \tag{24}$$

Here k_i and D_i are the overall mass-transfer coefficient and the axial dispersion coefficient of component i, respectively, and a_p is the specific surface area for adsorption. The last equation is coupled to the others through the equilibrium adsorbed concentration, which appears in the linear driving force model on the right hand side of Eq. (23).

The many simulations that have been carried out with such a model confirm the validity of the theoretical analysis presented above, particularly in identifying the typical separation regimes and in locating with a rather good approximation the corresponding separation regions in the operating parameter space (cf. Refs. [12,15] for a quantitative comparison between equilibrium theory results and detailed simulations in the case of isocratic SMBs).

In the following, this conclusion is supported by the discussion of the simulation results obtained for the α-ionone system mentioned above. In all simulations, $x_D = 0$ and $x_F = 0.5$, and the operating conditions are tuned in such a way that x_2 would always be equal to 0.34 in the equivalent SG-TMB unit. Accordingly, the topology of the separation regions shown in Fig. 9a and redrawn for the sake of convenience in a different scale in Fig. 13 applies. The SG-SMB unit is constituted of eight columns, arranged in a closed-loop 2-2-2-2 configuration. A complete set of Eqs. (22) to (24) above is used to describe each column, and the eight sets of partial differential equations are coupled through algebraic equations enforcing fulfillment of the overall and of the component material balances at the nodes of the unit. The following transport and column parameters have been adopted: $D_A = D_B = D_W = 0.001$ cm^2/s; $a_p k_{q,A} = a_p k_{q,B} = 10$ s^{-1}; $\varepsilon_b = 0.7$, and $\varepsilon_p = 0$. A switch time $t^* = 200$ s has been adopted in all simulations, whereas internal and external flow-rates have been adjusted so as to obtain different sets of m_j values.

In Table 1, the operating conditions and the simulation results obtained for the operating points A to I in Fig. 13 are shown. The first two columns report the values of x_2 and x_3 that have been

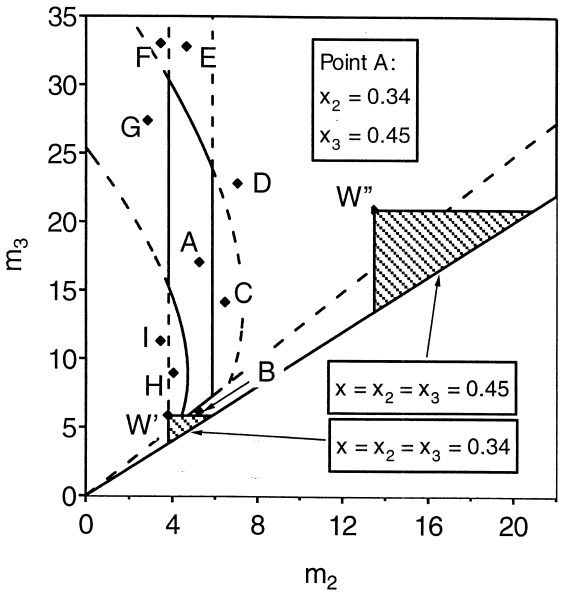

Fig. 13. SMB separation of the α-ionone enantiomers in methanol–water. Solvent gradient mode complete separation region for $x_2 = 0.34$, and $x_F = 0.5$ and $x_D = 0$; the broken lines define the regions attaining different separation regimes as illustrated in Fig. 9a. The hatched triangles are the isocratic complete separation regions for the mobile phase compositions as indicated in the figure. The operating points of the simulation runs in Tables 1 and 2 are also drawn.

calculated for the equivalent TMB unit. Then the m_j values ($j = 1, \ldots, 4$) are given, and finally the calculated extract and raffinate purities are indicated; these are defined as the solvent free average purity (in per cent) of A in the extract and of B in the raffinate, when the SMB cyclic steady state is achieved. If no purity value is indicated, this means that no solute is present in the corresponding outlet stream, i.e. that stream is flooded with mobile phase containing no solute. It can be readily observed that the calculated separation performance is fully consistent with the position of the operating point in the diagram. In particular, it is worth noting that in run C component A indeed accumulates in the unit, as predicted by our theoretical analysis, and that the same happens with component B in point H. Of course, this can happen since in the model the saturation either of the stationary phase or of the fluid phase is not accounted for, hence the solutes can indeed accumulate indefinitely in the unit.

Let us focus on the operating point A, where the theoretical internal mobile phase composition levels are $x_2 = 0.34$ and $x_3 = 0.45$, and complete separation of the two enantiomers has been achieved. In Fig. 13 also the two isocratic complete separation regions are drawn, which correspond to the two cases $x_D = x_F = x_2 = x_3 = 0.34$ (smaller hatched triangle below the SG-SMB complete separation region) and $x_D = x_F = x_2 = x_3 = 0.45$ (larger hatched triangle on the right hand side of the SG-SMB complete separation region). The operating conditions and the results of a few isocratic simulations are reported in Table 2; each run is identified by a letter, referring to the corresponding operating point in Fig. 13, and by either a prime or a double prime, indicating whether the mobile phase composition is $x = 0.34$ or $x = 0.45$, respectively. The m_1 and m_4 values have been chosen in such a way to fulfill the relevant constraints (8) and (11), respectively, namely $m_1 > H_A(0.34) = 5.85$ and $m_4 < H_B(0.34) = 3.82$ in runs A′, B′, C′, and H′, and $m_1 > H_A(0.45) = 20.9$ and $m_4 < H_B(0.45) = 13.5$ in run A″.

In run A′ only the extract is pure, but almost the whole feed is collected in the raffinate, where purity

Table 1
Solvent gradient SMB separation of the α-ionone enantiomers in methanol/water, operating conditions and calculated purity performance

Run	x_2	x_3	m_1	m_2	m_3	m_4	P_E	P_R
A	0.340	0.450	11.9	5.3	17.0	9.0	100	100
B	0.340	0.360	6.0	5.3	6.1	5.7	95	66
C	0.340	0.426	9.3	6.5	14.1	7.4	–	100
D	0.340	0.450	11.9	7.1	22.7	8.9	–	50
E	0.340	0.477	19.5	4.7	32.7	13.9	100	79
F	0.340	0.483	11.4	3.5	32.9	8.0	93	92
G	0.340	0.483	8.5	2.9	27.3	6.0	78	100
H	0.340	0.426	9.3	4.1	8.9	7.4	100	–
I	0.340	0.450	11.9	3.5	11.2	9.0	50	–

Table 2
Isocratic SMB separation of the α-ionone enantiomers in methanol/water, operating conditions and calculated purity performance

Run	$x_2 = x_3$	m_1	m_2	m_3	m_4	P_E	P_R
A′	0.340	9.4	5.3	17.0	3.0	100	51
A″	0.450	26.0	5.3	17.0	10.0	59	100
B′	0.340	9.4	5.3	6.1	3.0	100	79
C′	0.340	9.4	6.5	14.1	3.0	–	50
H′	0.340	9.4	4.1	8.9	3.0	100	61
W′	0.340	9.4	3.8	5.9	3.0	100[a]	100[a]
W″	0.450	26.0	13.5	20.9	10.0	100[a]	100[a]

[a] Assumed value, not calculated.

is only slightly larger than 51%. On the contrary, in run A″ only the raffinate is pure. In both cases the behavior is fully consistent with the relative position of point A in the (m_2, m_3) plane with respect to the small isocratic triangle at $x = 0.34$ in the case of run A′, and to the large isocratic triangle at $x = 0.45$ in the case of run A″. This proves that the solvent gradient operation makes indeed available for complete separation zones of the operating parameter space, which do not achieve complete separation in the isocratic case. Now, let us consider runs B′, and H′, where only the extract is pure, and run C′ where all the feed ends up in the raffinate product. The calculated behavior is again consistent with the relative position of the relevant operating points with respect to the isocratic triangle for $x = 0.34$. On the one hand, run B′ improves the performance of run B, since point B is below the critical regeneration line in the (m_2, m_3) plane in the solvent gradient mode, whereas in the isocratic mode there is no solvent balance constraint (13) on m_1 and m_4, and then these can be properly chosen to fulfill the corresponding separation constraints (8) and (11). On the other hand, runs C′ and H′ do not lead to accumulation of any component in the unit as it happens in the solvent gradient runs C and H; this is because this accumulation effect cannot occur in the isocratic mode. However, since $m_2 > H_A(0.34)$ in run C′, both components are collected only in the raffinate outlet and the extract is flooded with desorbent.

Thus, it has been shown how different the separation performance can be in the solvent gradient mode with respect to the isocratic mode for the same operating point in the (m_2, m_3) plane. Let us now evaluate the benefit in terms of separation performance that can be gained when operating a SG-SMB unit in the operating point corresponding to run A in Table 1, with respect to operating an isocratic SMB in the optimal vertices of the two isocratic triangles in Fig. 13, which are identified as runs W′ and W″ in Table 2. For the sake of simplicity, we assume that these two runs achieve 100% purity in both extract and raffinate, i.e. the same separation quality as in run A. Two performance parameters are considered, namely desorbent requirement and productivity [14,15]. The former is calculated as the ratio $(m_1 - m_4)/(m_3 - m_2)$. The latter is not very significant here since it is proportional to the feed concentration, which plays no role under the linear adsorption conditions studied in this work; a measure of productivity that can be used for comparison is provided by the difference $(m_3 - m_2)$, which is proportional to the feed flow-rate. First, it must be observed that both performance parameters are better in run W″ than in W′; in fact the productivity measure $(m_3 - m_2)$ is 7.4 and 2.1, respectively, whereas desorbent requirement is 2.2 and 3.0, respectively. However, it should be observed that the very large value of m_1 in run W″ calls for a smaller switch time than in run W′ to keep pressure drop under control (or for a larger column cross section to have the same linear velocity in the two cases); this has a negative effect on productivity that may compensate the difference in the figures given above. In run A the solvent gradient mode allows for a productivity, i.e. a value of $(m_3 - m_2)$, equal to 11.7, i.e. more than 50% larger than in run W″; at the same time desorbent requirement drops to 0.25, i.e. almost ten times less than in the same run W″. This high-performance is achieved with an m_1 value, which is only 25% larger than in run W′. It should be noted that as far as pressure drop is considered in the solvent gradient mode operation section 3 is limiting rather than section 1, since most often $m_3 > m_1$. These figures provide a quantitative assessment of the arguments that were used in the Introduction to motivate the implementation of the solvent gradient strategy.

It is worth underlying once more that the gradient mode operation has not been optimized at all; in fact point A may well be non-optimal, and the external mobile phase compositions that have been selected may well be not appropriate when the dependence of solubility, density, and viscosity on mobile phase composition is considered. However, the results reported above indicate that really significant performance improvements can be achieved when a SMB separation is operated in the solvent gradient mode. This possibility certainly deserves careful consideration and further investigation.

One limitation to this rather optimistic picture comes from the observation that the use of the solvent gradient operation mode may make the constraints coming from the solubilities of the solutes more strict. In fact, the condition $x_F > x_D$ implies that the feed, where the solute concentration is larger, is reacher in the weak solvent, and there-

fore the solute solubility is lower. This limitation depends of course on the specific separation under examination, and is of course absent in all those cases where solute solubility is not limiting.

8. Nomenclature

a_p	specific surface of the adsorbent particles (l/cm)
c	concentration (mol/l)
D	axial dispersion coefficient (cm^2/s)
H	Henry's constant (−)
k	parameter in Eq. (2) (−)
k_q	mass transfer coefficient in the lumped pore diffusion model (cm/s)
m	flow-rate ratio (−)
n	parameter in Eq. (2) (−)
q	adsorbed phase concentration (mol/l)
Q	volumetric fluid flow-rate (ml/min)
Q_s	volumetric solid flow-rate (ml/min)
t	time (s)
t^*	switch time (s)
V	volume of the column (ml)
x	volume fraction of solvent W in the fluid phase (−)
z	axial coordinate (cm)

Greek letters

ε^*	overall bed void fraction (−)
ε_b	bed void fraction (−)
ε_p	particle porosity (−)

Subscripts and superscripts

A	more retained component
B	less retained component
D	desorbent
E	extract
F	feed
i	component index ($i = A,B$)
j	section index ($j = 1..4$)
P	at operating point P
R	raffinate
SMB	Simulated Moving Bed
TMB	True Moving Bed
W	solvent W
0	reference value at $x = 0$

Acknowledgements

The partial support of ETH Zurich through grant TH-23′/00-1 is gratefully acknowledged.

References

[1] D.M. Ruthven, C.B. Ching, Chem. Eng. Sci. 44 (1989) 1011.
[2] R.-M. Nicoud, Pharm. Technol. Eur. 11 (1999) 28.
[3] M. Juza, O. Di Giovanni, G. Biressi, M. Mazzotti, M. Morbidelli, Trends Biotechnol. 18 (2000) 108.
[4] R.M. Nicoud, in: G. Subramanian (Ed.), Bioseparation and Bioprocessing, Wiley. VCH, New York, 1998.
[5] J.Y. Clavier, M. Perrut, R.M. Nicoud, in: Ph. Rudolf von Rohr, Ch. Trepp (Eds.), High Pressure Chemical Engineering, Elsevier, London, 1996.
[6] F. Denet, W. Hauck, R.M. Nicoud, M. Mazzotti, M. Morbidelli, Ind. Eng. Chem. Res. (2001) in press.
[7] M. Mazzotti, G. Storti, M. Morbidelli, J. Chromatogr. A 786 (1997) 309.
[8] O. Di Giovanni, M. Mazzotti, M. Morbidelli, F. Denet, W. Hauck, R.M. Nicoud, J. Chromatogr. A 919 (2001) 1.
[9] C. Migliorini, M. Wendlinger, M. Mazzotti, M. Morbidelli, Ind. Eng. Chem. Res. 40 (2001) 2606.
[10] T.B. Jensen, T.G.P. Reijns, H.A.H. Billiet, L.A.M. van der Wielen, J. Chromatogr. A 873 (2000) 149.
[11] D. Antos, A. Seidel-Morgenstern, Chem. Eng. Sci. (2001) submitted for publication.
[12] C. Migliorini, A. Gentilini, M. Mazzotti, M. Morbidelli, Ind. Eng. Chem. Res. 38 (1999) 2400.
[13] G. Storti, M. Mazzotti, M. Morbidelli, S. Carrla, AIChE J. 39 (1993) 471.
[14] M. Mazzotti, G. Storti, M. Morbidelli, J. Chromatogr. A 769 (1997) 3.
[15] G. Biressi, O. Ludemann-Hombourger, M. Mazzotti, R.M. Nicoud, M. Morbidelli, J. Chromatogr. A 876 (2000) 3.